Geophys. J. Int. (2000) **142,** 52–58

Characterization of experimental dynamos

Nicholas L. Peffley,[1] Alexei G. Goumilevski,[2] A. B. Cawthrone[1] and Daniel P. Lathrop[1]

[1] *Institute for Plasma Research and Department of Physics, University of Maryland, College Park,* MD 20742, *USA.*
E-mail: dpl@complex.umd.edu
[2] *Dynaflow, Inc.,* 7210 *Pindell Sch. Road, Fulton,* MD 20759, *USA*

Accepted 2000 January 14. Received 2000 January 10; in original form 1998 December 6

SUMMARY

Laboratory models of geophysical magnetic field production require new experimental characterization methods. Self-generating liquid metal magnetic dynamos are explored using two new experiments. Kinematic dynamo studies lead us to characterize the magnetic field dynamics in terms of eigenvalues and eigenfrequencies of the induction equation. Observing the decay of magnetic field pulses indicates the real part of the leading eigenvalue of the induction equation, while a chirp magnetic field diagnoses the imaginary part of the eigenvalue. Finally, a single-frequency applied magnetic field characterizes the structure of the velocity field. These measurements provide a new means to characterize and measure the approach to self-generation. We present data from numerical simulations and laboratory experiments using these techniques.

Key words: dynamos, experiments, liquid sodium, rotating convection.

1 INTRODUCTION

Questions about planetary magnetic field saturation, dynamics and the necessary geometry and forcing may soon be addressed by laboratory experiments. We wish to explore the dynamo mechanism where the motion of a conducting fluid generates the magnetic field. Although magnetic field self-generation in conducting liquid flows is a robust phenomena in nature, and despite much progress having been made in the theoretical and numerical studies of dynamo action, self-generation has not yet been observed in laboratory liquid metal experiments. Self-excited dynamos have been constructed using rotating disks, cylinders or wound rotors (Roberts & Jensen 1993; Wilkinson 1984). The attempt closest to achieving self-generation in a bulk liquid metal was performed by Gailitis *et al.* (1987). In their experiment, liquid sodium was pumped through a spiral channel to obtain the helical motion for a specific dynamo theoretical geometry. Measurements suggested that the system came to within 30 per cent of the threshold. Currently, several efforts to achieve experimental liquid metal dynamos are underway, in Karlsruhe, Riga, Paris, Madison and College Park. The efforts to build dynamo experiments necessitate the development of experimental and analytical techniques to characterize the transitions to self-generation in these systems. In this paper, we demonstrate experimental techniques appropriate for studying this transition. These techniques include pulse, single-frequency and multi-frequency (chirp) response measurements to imposed magnetic fields. We also provide an analysis of a single-frequency method by analytically and numerically examining the solutions of the induction equation at low magnetic Reynolds number.

The existing theories of a kinematic dynamo revolve around the induction equation for a magnetic field $\mathbf{B}$,

$$\frac{\partial \mathbf{B}}{\partial t} = \nabla \times (\mathbf{V} \times \mathbf{B}) + \eta \nabla^2 \mathbf{B}, \tag{1}$$

where $\mathbf{V}$ is the fluid velocity and $\eta = 1/\sigma\mu$ is the magnetic diffusivity, which is composed of the electrical conductivity σ and the magnetic permeability μ. This equation is derived from the Maxwell equations and Ohm's law for a moving conductor. Recast into dimensionless form, the equation is

$$\frac{\partial \mathbf{B}}{\partial t'} = R_m \nabla' \times (\mathbf{V}' \times \mathbf{B}) + \nabla'^2 \mathbf{B}, \tag{2}$$

where $R_m = UL/\eta$ for velocity scale U and length scale L, ∇ and $\mathbf{V}$ have been non-dimensionalized using these scales and t has been non-dimensionalized using the diffusive time L^2/η. The magnetic Reynolds number R_m characterizes the ratio of magnetic field advection due to conductor motion to magnetic field diffusion due to conductor resistivity. When diffusion dominates ($R_m \ll 1$), dynamo action is precluded. Previous difficulties in observing self-generating laboratory liquid metal dynamos stem partially from the small or modest R_m achieved. Because of advances in the fast breeder reactor program and the pioneering work of Gailitis *et al.* (1987), sodium handling has become more routine. The high electrical conductivity of sodium allows large R_m [$R_m \sim O(100)$] to be achieved in laboratory liquid metal dynamo experiments.

© 2000 RAS

The kinematic dynamo problem is as follows: given a prescribed velocity field, will a seed magnetic field grow in time (Moffatt 1978; Proctor & Gilbert 1994; Reyl 1996)? Numerical simulations using a number of different velocity fields have shown transition to self-generation when R_m is above a threshold value (Dudley & James 1989). It is assumed that before transition the Lorentz forces are weak and do not appreciably change the fluid velocity field. This paper applies ideas from the kinematic dynamo problem to develop and demonstrate experimental techniques for studying the transition to self-excitation.

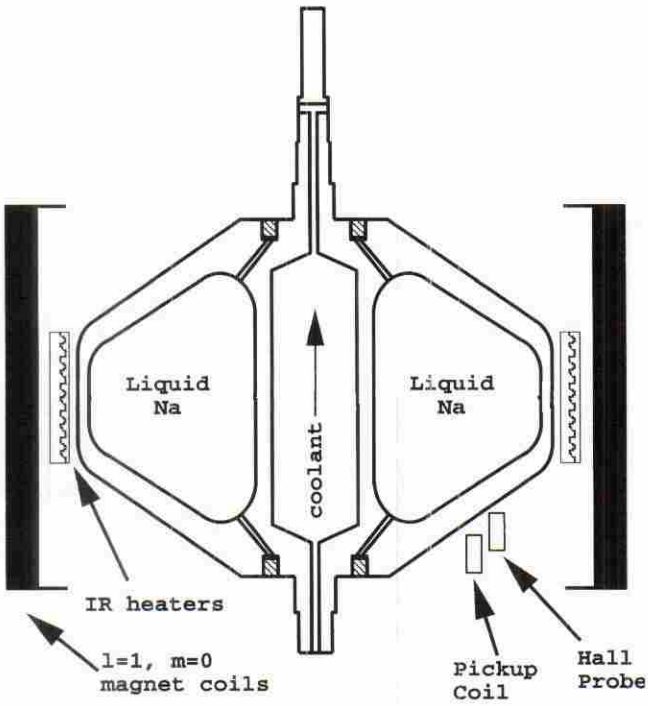

Figure 1. Cross-section of the rotating convection experiment. A titanium rotor contains 1.5 l of liquid sodium. A solenoid wound about the axis of rotation supplies excitation magnetic fields.

2 EXPERIMENTAL SET-UP

The development of the characterization techniques stems from our work on two dynamo experiments: a geophysically motivated rotating convection experiment and a mechanically forced experiment. The convection experiment (Fig. 1) consists of a 20.3 cm diameter titanium vessel containing 1.5 l of liquid sodium. This experiment is motivated by planetary convection such as is thought to occur in the Earth's outer core. The vessel is heated on the outer rim by quartz tungsten heaters and cooled along the axis by circulated hexane. The rotation causes centrifugally driven convection in the liquid sodium, where the centrifugal force replaces the gravitational force in planetary convection. The mechanically forced experiment is motivated by the work of Dudley & James (1989). The experiment (Fig. 2) consists of a hollow 30.5 cm diameter stainless steel sphere filled with 15 l of liquid sodium. Two counter-rotating stainless steel propellers, each powered by a 7.4 kW electric motor controlled by a variable frequency drive, provide mechanical pumping.

Both experiments use the same electronics for power control and data acquisition. A data acquisition computer and a delay pulse generator handle the timing of applied magnetic fields and data acquisition. An FFT network analyser allows us to examine signals from various sense coils, as well as providing both sine and chirp sources for applied magnetic fields. IGBT switches allow us to turn DC magnetic fields rapidly on and off, and a Hall probe allows us to measure the decay of these DC fields.

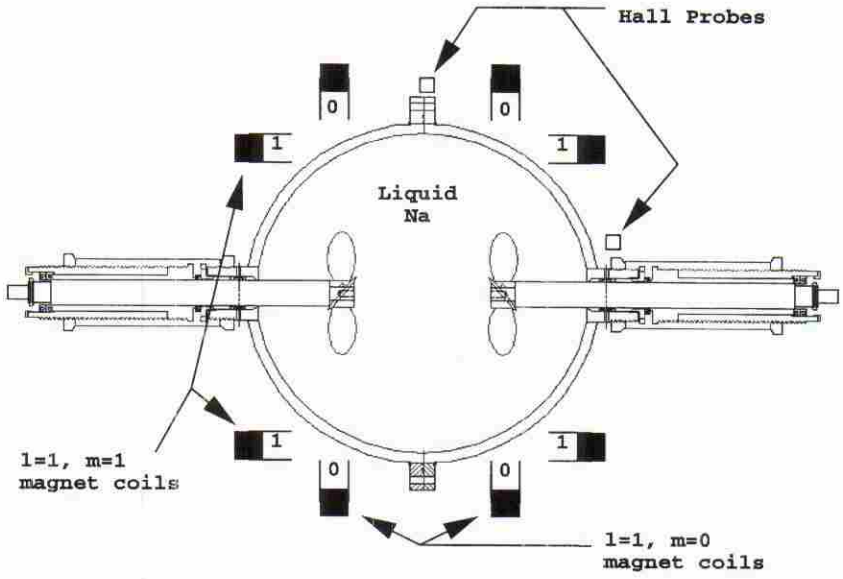

Figure 2. Cross-section of the mechanically forced experiment. Independently rotating shafts each drive propellers. The axial location of the propellers is adjustable. Each shaft is driven by a 7.5 kW motor controlled by variable frequency drives. Separate Helmholtz coil pairs supply excitation magnetic fields along the z-axis (dipole field with $m=0$, along the shaft axis) and along the x-axis (dipole field at right-angles to the shaft axis).

3 DECAY MEASUREMENT TECHNIQUES

The induction equation (eq. 1) may be solved as an eigenvalue problem for **B**, given the velocity field **V** (if **V** is stationary):

$$\mathbf{B} = \sum_{i=0}^{\infty} \exp(\lambda_i t) B_i(\mathbf{r}),$$

$$\lambda_i \mathbf{B}_i = \nabla \times (\mathbf{V} \times \mathbf{B}_i) + \eta \nabla^2 \mathbf{B}_i, \tag{3}$$

where λ_i–$\mathbf{B}_i$ are the eigenvalue–eigenvector pairs. Floquet theory allows similar treatment if **V** is periodic in time. For turbulent velocity fields, no exact solution is possible. Replacing **B** with the time-averaged velocity field in eq. (2) is perhaps a reasonable first approximation. The experiments of Gailitis *et al.* (1987) partially support this view. These eigenvalues and eigenvectors are functionals of the velocity field. For conditions below transition, the largest eigenvalue is negative and the decay time τ of the magnetic field is given by $\tau^{-1} = -\mathcal{R}e(\lambda_*) = -\max(\mathcal{R}e(\lambda_i))$. Measurements of the eigenvalue λ_* allow one to quantify the transition of a system from a damped state to a self-excited one. For a suitable velocity field and sufficiently large R_m, a positive $\mathcal{R}e(\lambda_*)$ occurs and small field perturbations grow exponentially in time (Moffatt 1978; Proctor & Gilbert 1994). The initial time dependence of the growing field will be set by the value of λ_*. Above transition, saturation of **B** will occur when the Lorentz force begins to modify the velocity field. This may cause steady, oscillatory, chaotic or turbulent magnetic fields reyl. A pulse measurement, which is specifically designed to study this transition, utilizes Hall effect magnetic field measurements in association with an external excitation coil. It can be used to determine how far the system is from the threshold magnetic Reynolds number. The measurement is performed by observing the decay rate of the magnetic field after an external DC field is applied and then rapidly turned off. The magnetic field will show an exponential decay due to induced eddy currents in the liquid metal and the conducting parts of the apparatus. With no velocity field, this phenomenon is the same as one sees in the decay of current and field in an LR circuit. The time constant τ can be estimated when $R_m = 0$ from the magnetic diffusion time, $\tau_d = L^2\eta^{-1}$, $\lambda_* \approx -\tau_d^{-1}$. If there are motions in the liquid metal that enhance field growth but are not strong enough to overcome resistive decay, the eigenvalue will shift towards zero. If we are above transition, the field will not decay at all. As the system passes transition, the value of the eigenvalue will pass through zero.

Fig. 3 shows a typical decay measurement taken from the mechanically driven experiment. Fig. 3(a) shows the full decay measurement, while Fig. 3(b) shows the semi-log plot of the pulse just after the applied field is turned off. A least-squares fit to the data gives the slope that is taken as an estimate of λ_{max}. As the system approaches transition to self-generation, one would see the pulse decay more slowly as λ_{max} approaches zero. After transition the field should grow exponentially until saturation.

An increasing (towards zero) eigenvalue has been measured for the mechanically forced system with magnetic fields pulsed in the z-direction (along the axes of the propellers). Fig. 4 shows the dependence of the eigenvalues on magnetic Reynolds number for a configuration with 12.7 cm propellers with 12.7 cm pitch, mounted with 15.3 cm between the propellers axially. Four 1.5-cm-wide baffles were placed running longitudinally in order to enhance flow towards the poles (poloidal flow). Since the eigenvalues should be sensitive to the geometry, measurements of the eigenvalue dependence on propeller position and propeller/impeller geometry are currently being performed.

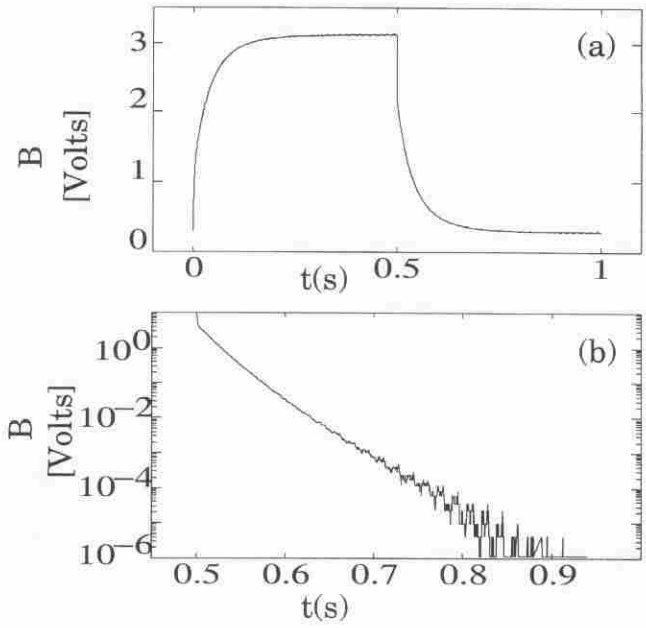

Figure 3. A pulse decay measurement is used to estimate the largest eigenvalue for the magnetic field dynamics. A Hall probe signal (a) indicates the magnetic field during the pulse. Analysis of the decay using a least-squares estimate of the slope (b) yields an eigenvalue estimate.

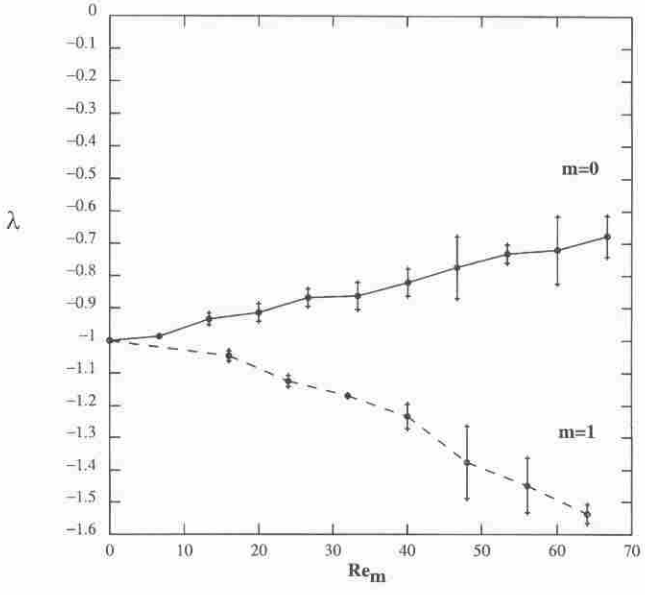

Figure 4. Variation of the decay eigenvalues (normalized by the unforced decay rate) for fields stimulated in the z-direction ($m = 0$, along the shaft axis) and the x-direction ($m = 1$) in the mechanically forced experiment. The $m = 0$ direction shows a trend towards self-generation, which would be achieved when $\lambda = 0$.

4 CHIRP MEASUREMENT TECHNIQUE

The chirp magnetic field excitation consists of exciting the system over a specific range of frequencies with equal power per frequency. In this way we measure the response of the liquid metal system to a large number of frequencies at once. This allows an evaluation of the imaginary part of the eigenvalue λ_*. The induced magnetic field will be amplified greatly at resonance, that is, when the excitation frequency coincides with the least damped frequency, $\omega_* = \mathcal{I}m(\lambda_*)$. This follows from the solution to eq. (2) in the presence of an external excitation at a frequency ω_0:

$$\mathbf{B} = \sum_{k=0}^{\infty} \left[\frac{C_k}{i\omega_0 - \lambda_k} \exp(i\omega_0 t) + D_k \exp(\lambda_k t) \right] \mathbf{B}_k(\mathbf{r}) . \tag{4}$$

Here ω_0 is the excitation frequency and C_k, D_k are constants associated with initial and boundary conditions.

Fig. 5 shows a typical chirp response measured using a pick-up coil attached just outside the case of the mechanically driven experiment. If the system approaches self-generation to an AC magnetic field, the chirp response would show a peak at that frequency, which would continue to grow as the system approaches transition. One can also use the chirp measurement to obtain $\lambda_{\max}$ for modes with zero imaginary part by measuring the chirp response as frequency approaches zero. Using a linear regression to find the magnitude at $\omega = 0$, one could obtain similar information to that obtained when measuring a system's response with a pulsed magnetic field.

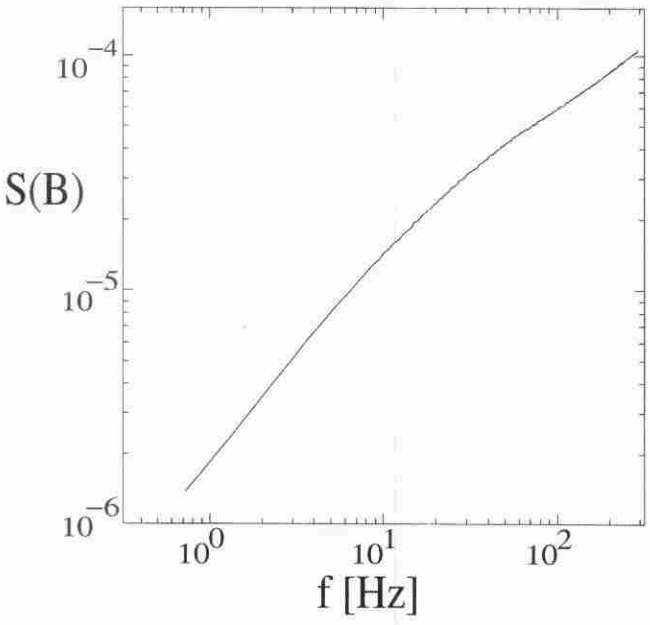

Figure 5. Power spectrum of the magnetic field in response to a chirp of imposed magnetic field. A synthesized signal containing components from 0.7 to 290 Hz is generated by an FFT network analyser. A power amplifier supplies that signal to an $l = 1$, $m = 0$ coil external to the dynamo experiment. A stationary coil detects magnetic fields exiting the system in response to this external perturbation. If the system approaches transition with a non-zero imaginary part of the leading eigenvalue, this diagnostic will show a peak forming at the characteristic frequency.

5 SINGLE-FREQUENCY DIAGNOSTIC

A single-frequency technique has been used to characterize the pattern of the liquid metal velocity field. The method consists of exciting the system with an external magnetic field at a single frequency and then measuring the spectrum of the response magnetic field exiting the system. In order to understand this measurement, we begin with the dimensionless induction equation (eq. 2). When $R_m \ll 1$, we can expand $\mathbf{B}$ in a convergent power series of R_m of the form

$$\mathbf{B} = \sum_{k=0}^{\infty} \mathbf{B}_k R_m^k . \tag{5}$$

Because eq. (2) is linear in $\mathbf{B}$, the equations of motion to first order reduce to

$$\frac{\partial \mathbf{B}_0}{\partial t} = \nabla^2 \mathbf{B}_0 , \tag{6}$$

$$\frac{\partial \mathbf{B}_1}{\partial t} = \nabla \times (\mathbf{V} \times \mathbf{B}_0) + \nabla^2 \mathbf{B}_1 . \tag{7}$$

We can interpret $\mathbf{B}_0$ as the field produced by the excitation coils permeating the system. $\mathbf{B}_1$ is the first-order response field due to the velocity advecting $\mathbf{B}_0$.

In the rotating convection experiment, the strong rotation will organize the flow with respect to the axis of rotation. One measure of this is the Ekman number, $E = \nu/2\Omega L^2$, which characterizes the balance of viscous to Coriolis forces. Typical Ekman numbers in our rotating convection experiment are $E = 4 \times 10^{-7}$–5×10^{-8}, indicating a strongly rotating state. Such flows often exhibit geostrophic balance (Busse 1970) and organize into flow patterns independent of the direction aligned with the axis of rotation. Simple convective patterns take the form of Taylor columns (vortices aligned with the z-axis) with m-fold azimuthal symmetry. In the laboratory frame this rotating m-fold pattern yields frequencies of $m\Omega$. The $\nabla \times \mathbf{V} \times \mathbf{B}$ term in eq. (7) will generate beats of frequency $m\Omega \pm \omega$ that are seen in the spectrum of the magnetic field as measured by a pick-up coil. Similarly, an applied external DC field will produce frequencies of $m\Omega$.

Although the experiment has $R_m \sim 1$, we expect the previous analysis of the induced field in eqs (5)–(7) to provide insight into velocity structures in the experiment, as long as the system is below the transition to self-generation. Fig. 6 shows two spectra from a pick-up coil just outside the rotating convection experiment. The spectra show data at a rotor speed of $\Omega/2\pi = 98$ rps and an applied field excitation frequency of $\omega = 60$ Hz. The top graph shows the experiment with a temperature drop $\Delta T \sim 17$ °C, while the bottom graph has $\Delta T \sim 22$ °C. One expects the complexity of the convection to increase with increasing ΔT. Both graphs contain peaks at ω, while only at the smaller temperature difference do we observe peaks at $m\Omega$ ($m = 2$ and 4 are prominent) and $m\Omega \pm \omega$. This can be interpreted as showing two pairs of roll structures at $\Delta T \sim 17$ °C, while at $\Delta T \sim 22$ °C the state appears turbulent with no well-defined roll pattern.

We consider some analytical and numerical analyses to understand this technique further. It is useful to idealize the geometry for these analyses. We consider a cylindrical annulus of height H filled with a liquid and rotating with an angular velocity Ω about its vertical axis. We use eqs (5), (6) and (7) for

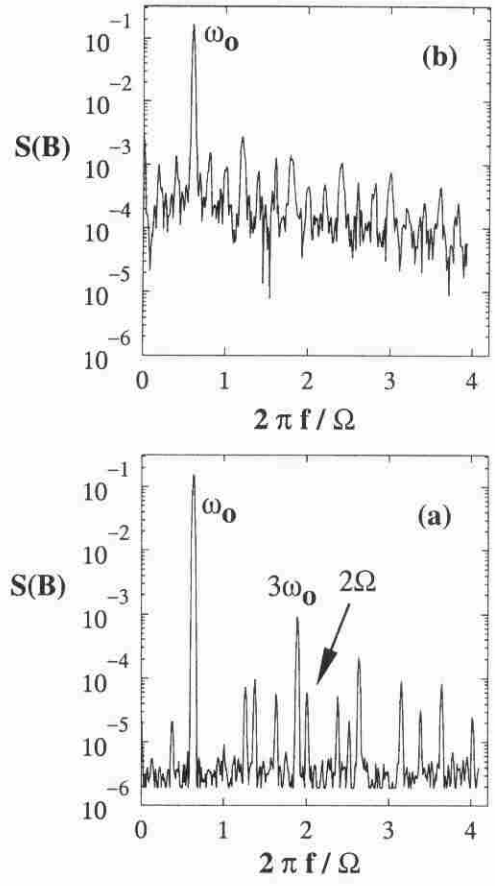

Figure 6. Spectra of the magnetic field fluctuations while the system is excited by a single frequency (60 Hz). The rotor was driven at a rotation rate of $\Omega/2\pi = 98$ Hz. Peaks at sum and difference frequencies are observed in (a) where $\Delta T = 17$ °C. Broad-band spectra indicative of turbulent convection in appear in (b) where $\Delta T = 22$ °C.

the induction equation expanded for small magnetic Reynolds number. The linearity of eq. (1) allows one to rewrite eq. (7) for higher-order $\mathbf{B}_k$:

$$\frac{\partial \mathbf{B}_k}{\partial t} = \boldsymbol{\nabla} \times (\mathbf{V} \times \mathbf{B}_{k-1}) + \nabla^2 \mathbf{B}_k . \tag{8}$$

Eq. (6) should be supplemented by a boundary condition that is determined by the configuration of the experimental set-up. With an applied external magnetic field, harmonic in time and aligned parallel to the axis of rotation, eq. (6) has a solution of the form

$$\mathbf{B}_0 = B_* \hat{e}_z e^{-i\omega_0 t} \left(\frac{J_0(r\sqrt{i\omega_0})}{J_0(\sqrt{i\omega_0})} \right), \quad \zeta \le r \le 1, \quad |z| \le h . \tag{9}$$

Here J_0 is the zeroth-order Bessel function, ω_0 is the frequency of excitation, $\hat{e}_z$ is the unit vector in the z direction and B_* is the amplitude of the external field. h, r and ζ are the height, radius and inner cylinder radius, respectively, where the outer cylinder radius is taken to be 1.

Eq. (7) is a diffusion equation with a source term

$$\mathbf{Q} = (\mathbf{B}_0 \cdot \boldsymbol{\nabla})\mathbf{V} - (\mathbf{V} \cdot \boldsymbol{\nabla})\mathbf{B}_0 . \tag{10}$$

This can easily be solved provided the Green's functions for the diffusion equation and the velocity field are known. A simple vortical velocity field consistent with geostrophic balance is

$$\mathbf{V} = m^{-1} \boldsymbol{\nabla} \times (\hat{e}_z P_{m,n}), \tag{11}$$

$$P_{m,n} = \exp(-im\phi) \sin(\gamma_n (r - \zeta)) . \tag{12}$$

Here, $\gamma_n = \pi n (1-\zeta)^{-1}$ is the radial wavenumber, n, m are the radial and azimuthal numbers and V_0 is the velocity amplitude of a columnar roll. The geostrophic velocity is expressed in the rotating frame of reference. To satisfy non-slip boundary conditions at the top and bottom of the annulus, the geostrophic velocity should be modified by Ekman layers (Zhang & Busse 1975; Busse & Carrigan 1974; Carrigan & Busse 1983).

Because of the two-dimensionality of $\mathbf{V}$, the magnetic field $\mathbf{B}_1$ is aligned parallel to the vertical axis $\hat{z}$. It is convenient to take the temporal Fourier transform of eq. (7) using eq. (11) for the velocity field,

$$\left(\frac{1}{r} \partial_r r \partial_r - \frac{m^2}{r^2} + i\omega \right) \hat{B}_1 = \sqrt{i\omega}\, \hat{Q}_\omega ,$$

$$\hat{Q}_\omega = B_* e^{im\phi} \hat{V}_r(\omega + \omega_0) \left(\frac{J_1(r\sqrt{i\omega_0})}{J_0(\sqrt{i\omega_0})} \right) . \tag{13}$$

Eq. (13) represents an example of the Sturm–Liouville problem, which has a solution satisfying homogeneous boundary conditions of the form

$$\begin{aligned} \hat{B}_1 &= \left(\frac{\pi}{2} \right) \left(\sqrt{\frac{\omega_0}{\omega}} \right) \Psi_1(r, \omega), \quad |z| \le h , \\ \Psi_1(r, \omega) &= \left(\frac{Y_1(r)}{Y_1(\zeta)} \right) \int_\zeta^r \hat{Q}_\omega(\xi) Y_2(\xi) d\xi \\ &\quad - \left(\frac{Y_2(r)}{Y_2(1)} \right) \int_r^1 \hat{Q}_\omega(\xi) Y_1(\xi) d\xi , \\ Y_1 &= J_m(\sqrt{i\omega}r) N_m(\sqrt{i\omega}) - N_m(\sqrt{i\omega}r) J_m(\sqrt{i\omega}) , \\ Y_2 &= N_m(\sqrt{i\omega}r) J_m(\sqrt{i\omega}\zeta) - J_m(\sqrt{i\omega}r) N_m(\sqrt{i\omega}\zeta) . \end{aligned} \tag{14}$$

Here J_m and N_m are the Bessel and Neumann functions of order m. In the laboratory frame $\phi \to \phi + \Omega t$, so the velocity field associated with the convection rolls is a harmonic function of the frequency. Therefore, $\hat{V}_r(\omega + \omega_0) \sim \delta(\omega + \omega_o - m\Omega)$ (where δ is the Dirac delta function). Performing an inverse Fourier transform, the magnetic field $\mathbf{B}_1$ is found to be

$$\mathbf{B}_1 = \left(\frac{\hat{e}_z}{4} \right) e^{-im\phi}\, e^{i(m\Omega - \omega_0)t} \left(\sqrt{\frac{\omega_0}{m\Omega - \omega_0}} \right) \Psi_1(r, m\Omega - \omega_0) . \tag{15}$$

The rotation of fluid introduces a novel feature: the frequency of oscillation of the induced magnetic field $\mathbf{B}_1$ differs from the excitation frequency of the external field. This shift in frequency is a product of the number of vortices in azimuthal direction m and the speed of rotation Ω. Therefore, the magnetic field $\mathbf{B}_1$ is characterized by well-pronounced spectral components at frequencies $\omega_0 \pm m\Omega$. Similarly, the second-order magnetic field, $\mathbf{B}_2$, is characterized by spectral components at frequencies $\omega_0 \pm 2m\Omega$, and so on. Thus, the general form of solution for the field $\mathbf{B}_k$ is

$$\mathbf{B}_k = \frac{\hat{e}_z}{4} e^{-ikm\phi}\, e^{i(km\Omega - \omega_0)t} \left(\sqrt{\frac{\omega_0}{km\Omega - \omega_0}} \right) \Psi_k(r, km\Omega - \omega_0) . \tag{16}$$

Here the function Ψ_k is given by eq. (14) with the Bessel and Neumann functions of order m replaced by the functions of order km.

We observe that in contrast to the axisymmetric field $\mathbf{B}_0$, the induced magnetic field $\mathbf{B}_1$ is a periodic function of angular variable ϕ. Using asymptotic properties of Bessel and Neumann functions, the magnitude of $\mathbf{B}_1$ can be estimated as:

$$\omega_0 \gg 1 : B_1 \sim (r-\zeta)(1-r)\exp[-(1-r)\sqrt{|\omega_0 - m\Omega|/2}],$$

$$\omega_0 \ll 1 : B_1 \sim (r-\zeta)(1-r)\omega_0 . \qquad (17)$$

At low values of the excitation frequency, $\omega_0 \ll 1$, the induced field $\mathbf{B}_1$ is symmetric with respect to the circumference $\hat{r} = (1+\zeta)/2$. At high values of the excitation frequency, $\omega_0 \gg 1$, the induced field is expelled from the inner region of the annulus and concentrates in a thin outer region. The thickness of the magnetic field penetration is given by $\delta = \sqrt{2|\omega_0 - m\Omega|^{-1}}$. This example demonstrates the well-known effect of magnetic field expulsion by a fluid flow with closed streamlines (Moffatt 1978).

Fig. 7 illustrates the results of simulations of the magnetic field B_1. These results were obtained by numerically integrating eq. (13), where the velocity field was given by eqs (11) and (12). The number of vortices in the azimuthal direction was $m = 6$, and in the radial direction, $n = 1$. The plots of B_1 were calculated for the following parameters: the speed of rotation, $\Omega_0 = 1$ Hz; the excitation frequencies, $f_0 = 1$, 5, 10, 30 Hz, the magnetic diffusivity of a fluid (liquid sodium), $\eta = 800$ cm^2/s, the apparatus length scale, $R_0 = 10$ cm; and the ratio of the inner radius to the outer radius, $\zeta = 0.3$. The dependence of the averaged magnetic field, $< B_1 >$, on the excitation frequency, $f_0 = \omega_0/2\pi$, is shown in Fig. 8.

Finally, Fig. 9 illustrates the distribution of B_1 over the cross-sectional area of the annulus for the excitation frequency $f_0 = 80$ Hz. This figure shows that the induced magnetic field concentrates near the outer boundary of the annulus, and the field is weak in regions of strong convection velocity and strong in regions of weak velocity. One can infer from this figure that the number of 'islands' of the magnetic field is the same as the number of columnar rolls, $m = 6$. By analogy, the second-order field, B_2, is characterized by $2m$ 'islands', the third-order field, B_3, by $3m$ 'islands', and so on. For moderate magnetic Reynolds numbers, $R_m \sim 1$, this circumstance makes the distribution of the induced magnetic field complex.

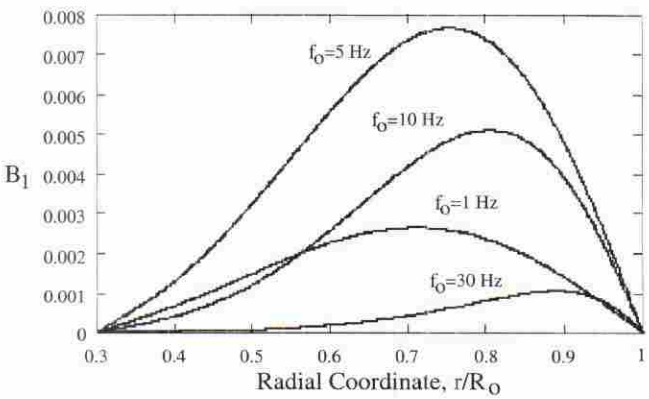

Figure 7. Theoretical distribution of the induced magnetic field due to a system of vortices B_1/B_0 with radial coordinate. The rotation rate is $\Omega/2\pi = 1$ Hz.

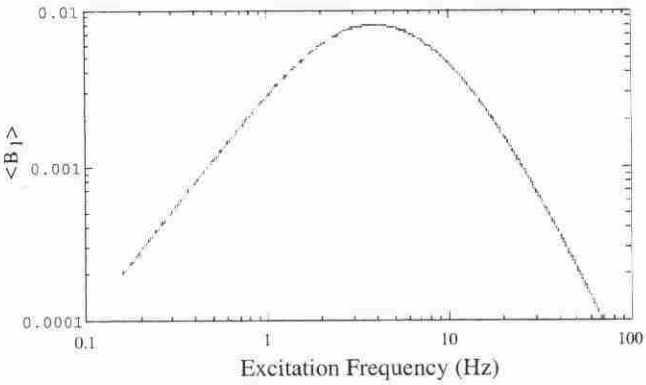

Figure 8. The theoretical dependence of the magnetic field averaged over the cross-sectional area of the annulus, $< B_1 > = 2B_0^{-1}(1-\zeta^2)^{-1}\int_\zeta^1 r|B_1(r)|dr$ on the excitation frequency, f_0. The speed of rotation of the fluid is $\Omega_0/2\pi = 1$ Hz.

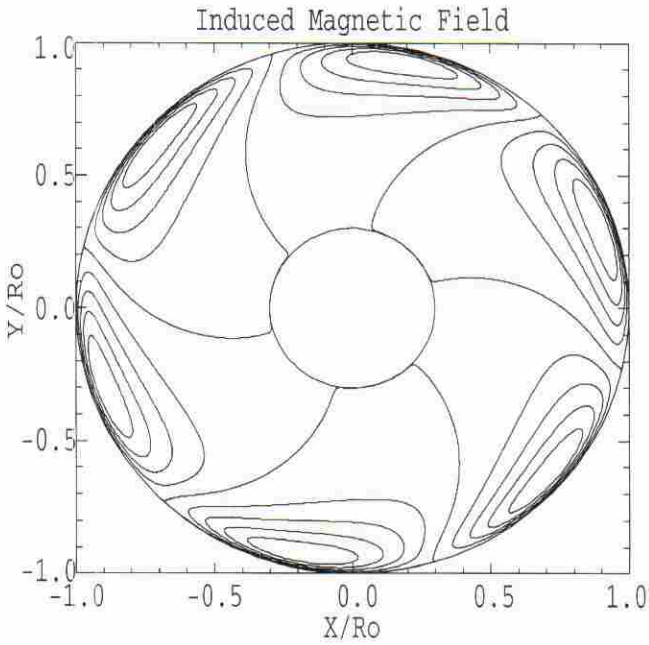

Figure 9. The theoretical isolines of the induced magnetic field, B_1, calculated for an excitation frequency $f_0 = 80$ Hz and a speed of rotation $\Omega/2\pi = 1$ Hz.

6 CONCLUSIONS

We have presented three techniques for characterizing laboratory geophysical liquid metal flows designed to achieve dynamo action. The pulse and chirp measurements are useful to indicate the leading eigenvalue for the magnetic field as one approaches transition. Single-frequency measurements are used to diagnose the structure of the velocity field. It is our hope that these techniques will be useful to the many experimental groups working on this challenging problem.

ACKNOWLEDGMENTS

We are grateful to Jim Drake, Edward Ott, Paul Roberts and Edward Bolton for helpful discussions, and acknowledge the support of the National Science Foundation under grants

EAR-9615789, EAR-9903958, EAR-9903162 and DMR-9701980. DPL is a Cottrell Scholar of the Research Corporation.

REFERENCES

Busse, F.H., 1970. Thermal instabilities in rapidly rotating systems, *J. Fluid Mech.*, **44,** 441–460.

Busse, F.H. & Carrigan, C.R., 1974. Convection induced by centrifugal buoyancy, *J. Fluid Mech.*, **62,** 579–592.

Carrigan, C.R. & Busse, F.H., 1983. An experimental and theoretical investigation of the onset of convection in rotating spherical shells, *J. Fluid Mech.*, **126,** 287–305.

Dudley, M.L. & James, R.W., 1989. Time-dependent kinematic dynamos with stationary flows, *Proc. R. Soc. Lond.*, **A425,** 407–429.

Gailitis, A.K., Karasev, B.G., Kirillov, I.R., Lielausis, O.A., Luzhanskii, S.M. & Ogorodnikov, A.P., 1987. Experiment with a liquid-metal model of an MHD dynamo, *Magnetohydrodynamics,* **23,** 349–353.

Moffatt, H.K., 1978. *Magnetic Field Generation in Electrically Conducting Fluids,* Cambridge University Press, Cambridge.

Proctor, M.R.E. & Gilbert, A.D., 1994. *Lectures on Solar and Planetary Dynamos,* Publications of the Newton Institute, Cambridge University Press, Cambridge.

Reyl, C., Antonsen, T.M. & Ott, E., 1996. Quasi-two-dimensional dynamo instabilities of chaotic fluid flows, *Phys. Plasmas,* **3,** 2564–2578.

Roberts, P.H. & Jensen, T.H., 1993. Homogeneous dynamos: theory and practice, *Phys. Fluids B,* **5,** 2657–2662.

Wilkinson, I., 1984. The contribution of laboratory dynamo experiments to our understanding of the mechanism of generation of planetary magnetic fields, *Geophys. Surv.*, **7,** 107–122.

Zhang, K.-K. & Busse, F.H., 1975. A model of the geodynamo, *Geophys. J. R. astr. Soc.*, **42,** 437–459.